IEEE Access
Multidisciplinary | Rapid Review | Open Access Journal

Received October 22, 2020, accepted November 7, 2020, date of publication November 16, 2020,
date of current version November 27, 2020.

Digital Object Identifier 10.1109/ACCESS.2020.3038307

On the Coexistence of Aperiodic and Periodic Traffic in Cellular Vehicle-to-Everything

LUCA LUSVARGHI[1], (Graduate Student Member, IEEE), AND MARIA LUISA MERANI[1,2], (Senior Member, IEEE)

[1]Dipartimento di Ingegneria "Enzo Ferrari," Università degli Studi di Modena e Reggio Emilia, 41125 Modena, Italy
[2]Consorzio Nazionale Interuniversitario per le Telecomunicazioni (CNIT), 43124 Parma, Italy

Corresponding author: Luca Lusvarghi (luca.lusvarghi5@unimore.it)

This work was supported by the Università degli Studi di Modena e Reggio Emilia, Italy, through the FAR 2019 Research Grant.

ABSTRACT Cellular Vehicle-to-Everything (C-V2X) communications are the key to connected and autonomous driving, and pave the way for future Intelligent Transport Systems (ITS). To support non-safety and safety critical applications in the demanding out-of-coverage scenario, the 3rd Generation Partnership Project (3GPP) has standardized the distributed C-V2X Mode 4 solution, whose behavior has been thoroughly analyzed for periodic traffic. In the current work, the problem of allocating aperiodic traffic in Mode 4 is tackled, a matter that has not been addressed before and that raises several challenging questions. A solution for serving such traffic type is put forth, and an analytical insight on the attainable performance is offered. Further, it is numerically proved that guaranteeing aperiodic flows good service levels is hard when their packets are not small sized. This holds true even for sophisticated physical layer choices and at relatively modest traffic densities, revealing that novel approaches to radio resource assignment are a necessity in Fifth Generation (5G) vehicular communications.

INDEX TERMS C-V2X, aperiodic vehicular traffic, vehicular communications, 5G.

I. INTRODUCTION AND STATE OF THE ART

Two alternative radio technologies are currently competing for vehicular communications, namely, Cellular Vehicle-to-Everything (C-V2X) and Dedicated Short Range Communications (DSRC). 3GPP standardized C-V2X in Release 14, defining two Vehicle-to-Vehicle (V2V) operating modes termed Mode 3 and Mode 4, for in-coverage and out-of-coverage scenarios, respectively. DSRC is the older contender, whose layer 1 and 2 specifications stem from the 802.11 domain, with only slight modifications. The two technologies are expected to coexist on the market, achieving different penetration degrees in distinct world regions: DSRC-based vehicular communications are already popular in the US, in Japan and to a less extent in Europe; C-V2X is rising a significant attention in China. C-V2X supporters advocate that the evolutionary path of cellular communications, transiting from LTE to 5G, will guarantee a long-term solution to road communications; furthermore, it will allow telco industries to offer connectivity services to one of the most attractive 5G "verticals", i.e., to the automotive realm. Hence, even though C-V2X is still facing many challenges, like the current scarcity of experimental deployments, as well as the uncertainty about its effectiveness in coping with congestion, yet it keeps gaining momentum day after day.

In C-V2X, Mode 4 is particularly interesting and represents the object of this investigation. Such mode supports direct vehicular communications without any need for network supervision; it can therefore operate in out-of-coverage conditions and results perfectly suited for safety applications. Mode 4 rests on a distributed Sensing-based Semi-Persistent Scheduling (SSPS) algorithm in which each vehicle selects transmission resources in an autonomous and distributed manner. The SSPS constituent procedures rely on the assumption of periodic and predictable traffic, such as the Cooperative Awareness Messages (CAMs), conveying basic information about vehicle status [1].

As of today, several works have thoroughly investigated SSPS performance in the presence of periodic packet transmissions. In [2], Masegosa *et al.* assessed the system-level behavior of C-V2V Mode 4 in a Manhattan grid urban topology, comparing it against that of a random scheduling strategy. In [3], Bazzi *et al.* provided an accurate analysis of the impact that different Medium Access Control (MAC) and

The associate editor coordinating the review of this manuscript and approving it for publication was Zhenyu Zhou.

physical layer parameters have on Mode 4 when the periodic CAM dissemination is targeted. The authors of [4] proposed a novel solution to combat the hidden terminal problem that affects the SSPS algorithm, whereas [5] highlighted the positive effects of full-duplex radios on Mode 4; these studies too, considered periodic traffic only.

Yet, the hypothesis of periodic CAM messages has been questioned through experimental data [6], and new models have been very recently introduced to generate realistic, non-cyclic CAM traces [7]. Moreover, enhanced V2X (eV2X) use cases foresee a mixture of periodic and *aperiodic* traffic, the latter being expected to display: (i) persistent transmissions for non-negligible times; (ii) non-deterministic interarrival times. Indeed, information detected through on-board cameras, either at low or high resolution, objects identified via lidars or radars, and shared through V2V, all generate flows that are stochastic in nature. To serve such heterogeneous traffic types, 3GPP Release 16 is required to introduce significant novelty in the forthcoming set of 5G vehicular communication specifications, named New Radio (NR)-V2X, presumably disclosed by the end of 2020.

This work is a first step towards NR-V2X investigations, as it addresses the key question of how to accommodate aperiodic, persistent traffic in legacy Mode 4. To the authors' knowledge, this is an aspect that has not been investigated in literature before and it is therefore worth being explored. A novel strategy to jointly serve periodic and aperiodic flows is proposed, under the design constraint of preserving the performance of periodic flows; indeed, Mode 4 was originally designed for it. The underlying assumption is that the interarrival time between aperiodic packets is a constant plus an exponentially distributed random time.

In [8], the same authors of the current paper analyzed the effectiveness of Mode 4 for multi-hop delivery of asynchronous Decentralized ENvironmental Messages (DENMs), in the presence of background, periodic CAM traffic. A similar issue was studied in [9], considering the benefit of short term sensing. However, DENMS are by no means comparable to stochastic packet transmissions; how to handle aperiodic flows deserves a proper investigation, that the present work initiates. It is also worth highlighting that the joint deployment of large data sets and machine learning represents an attractive approach to forecast aperiodic traffic, to be explored in the future; in this respect, the work in [10] offers a comprehensive survey on big data as a powerful enabler for the Internet of Vehicles. The same holds for energy-efficient resource allocation algorithms for vehicular networks, as those proposed in [11]. Unlike [10] and [11], this study is centered on the current 3GPP standard for V2V communications and it scouts whether some modifications to Mode 4 consent to tailor this communication mode to the requirements of aperiodic flows.

In detail, this work considers a physical layer model for V2V communications compliant to the NR specifications of 3GPP Release 15, that Release 16 NR-V2X will inherit. Extensive simulations are performed, to assess the performance guaranteed to aperiodic and periodic traffic, exploiting an enhanced version of the custom C-V2X ns-3 module introduced in [8]. The setting of the investigation is a highway trunk, that replicates the highway scenario defined in [12]; vehicle mobility is modeled through the widely adopted Simulation of Urban MObility (SUMO) traffic package. Standard 3GPP metrics are determined, for different percentages of vehicles generating aperiodic traffic, for different sizes and arrival rates of aperiodic packets, and for increasing vehicular densities.

The main contributions the current paper provides can be summarized as follows:

- The issue of coping with aperiodic flows in Mode 4 is faced and a simple, standard compliant approach is put forth;
- The throughput of the proposed resource allocation technique is analytically determined in the absence of transmission impairments, for the limiting case of aperiodic traffic only. The analysis outcomes are then used to forecast what to expect in a realistic vehicular scenario, when periodic flows are also present;
- the comparison between the proposed solution and two schemes that accommodate aperiodic traffic in accordance to SSPS is offered, providing numerical evidence of the superiority of the new strategy;
- It is analytically proved and verified by simulation that the performance of aperiodic traffic is insensitive to different latency requirements set for aperiodic packets;
- It is demonstrated that aperiodic users experience low performance levels, even when moderate traffic densities are examined, unless very small aperiodic packets are considered;
- 5G physical layer features alone are not enough to boost performance, when the Orthogonal Frequency Division Multiplexing (OFDM) numerology is set to 15 kHz, the lowest possible value.

The remainder of the paper is organized as follows: Section II provides an overview of the 3GPP Release 16 enhancements that are under discussion, whereas Section III recalls the main features of current C-V2X standard and Mode 4. Section IV tackles the problem of allocating radio resources to aperiodic traffic and proposes a reservation-less, Mode 4-based solution, along with its analytical model. Section V describes the simulation framework and the 5G physical layer implementation of the V2V communication channel. Section VI presents the numerical results and lastly, Section VII draws the concluding remarks.

II. PRINCIPLES OF NR-V2X COMMUNICATIONS

In recent years, the 5G Ultra Reliable and Low Latency Communications (URLLC) vision has stretched to include connected vehicle applications. As a matter of fact, 3GPP Release 15 introduced enhanced V2X (eV2X) applications such as vehicle platooning, extended sensors, remote and advanced driving [13], characterized by very demanding

latency, reliability and data rate requirements. As a consequence, a great deal of activity is currently ongoing within the 3GPP working groups to finalize the new V2X standard. Its novel communication solutions have to successfully serve the challenging eV2X use cases portrayed in Release 15. Further, they have to cope with mixed traffic scenarios where aperiodic and periodic flows coexist, accommodating unicast and groupcast communications. This unprecedented adaptability will be powered by significant changes in the physical (PHY) layer and the MAC sublayer.

From the PHY layer standpoint, [14] pointed out that direct V2V communications will mostly inherit the standardized 5G NR features of cellular uplink channels. In the sub-6 GHz band, NR-V2X is expected to adopt Cyclic Prefix (CP)-OFDM waveforms with scalable numerologies, employing 15 kHz, 30 kHz and 60 kHz subcarrier spacings. Moreover, NR-V2X will employ Low Density Parity Check (LDPC) codes for the data channel and CRC-assisted polar codes for the control channel, supporting higher order modulation schemes and Multiple-Input Multiple-Output (MIMO) antenna geometries. Within the MAC sublayer, NR-V2X will feature two new resource allocation modes, Mode 1 and Mode 2, to replace legacy Mode 3 and Mode 4, respectively.

Mode 2 collectively points at solutions that assign no role to the next generation NodeB (gNB) in the resource allocation process, guaranteeing reliable communications in out-of-coverage scenarios as Mode 4 does. The goal is to devise techniques that warrant immediate and reliable access to transmission resources, combined with fast repetitions, if needed. According to the proposal in [15], Mode 2 will presumably encompass an approach where vehicles are pre-configured with a pool of Time-Frequency Resource Patterns (TFRPs) that indicate the time and frequency location for each repetition of the Transport Block (TB), i.e., the PHY layer data unit carrying the packet. Every time a new packet is generated, the transmitting vehicle will either select a single time-frequency resource (as in Mode 4), or identify the TFRP for the initial transmission and the subsequent retransmissions of the TB. However, since NR-V2X will have to cope with both aperiodic and periodic traffic, there is a lack of consensus on whether the periodic resource reservation of Mode 4 should be included in NR-V2X. For instance, [15] argued that removing the periodic reservation feature might lead to less effective communications in some circumstances.

An additional question to address is how to perform the sensing and selection procedure in NR-V2X Mode 2. As reported in [15], the building blocks of the sensing mechanism are expected to be the same as in SSPS. Exploiting the information gathered during the sensing window, each vehicle builds its own list of candidate radio resources, filters it according to some thresholds and then randomly selects one resource out of the refined list, in that closely resembling C-V2X Mode 4 operations. The rapporteurs in [15] stated that Mode 2 does not have to be complemented by any short-term sensing technique (i.e., listen-before-talk), as this choice is likely to increase energy consumption and system complexity. On the opposite rim, the document in [16] pointed out that full-duplex enabled short-term sensing significantly helps in reducing collision occurrences when both periodic and aperiodic traffic coexist, and allows the implementation of a Quality of Service (QoS)-based access policy.

To further testify how open the discussion is, an alternative Mode 2 sensing procedure appeared in [17], consisting in a geographic information-based dynamic TFRP mapping. A parallel 3GPP document by the same authors also investigated the resource allocation problem of aperiodic traffic with variable packet size, proposing to segment the aperiodic packet in multiple Transport Blocks (TBs), the first transmitted without reservation and the remaining TBs allocated in reserved resources [18].

To date, the allocation of aperiodic traffic is still lacking the definitive solution; within 3GPP working groups, one proposal interestingly indicates that, to support aperiodic and bursty traffic, in some situations the vehicle may perform a one-time transmission without periodic reservations [15]. This represents the starting point of the current study. Moreover, given that it seems likely that some Mode 4 traits will be inherited by NR-V2X, the current work focuses on such mode, to determine whether it can be tailored to meet the needs of both periodic and aperiodic vehicular traffic sources.

III. SIDELINK V2V IN RELEASE 14

A. MODE 3 AND MODE 4

In Release 14, two distinct modes are standardized to accommodate V2V communications, named Mode 3 and Mode 4. In Mode 3, the Evolved Node B (eNB) is in charge of coordinating the dynamic assignment of radio resources to all vehicles, therefore avoiding conflicts. The standard does not indicate a specific resource management algorithm, it is up to each cellular operator to design and implement its own. However, the eNB central orchestration requires all vehicles to be under cellular coverage, a condition clashing with the requirements of safety applications, that cannot depend on the availability of such coverage. On the other hand, in Mode 4 vehicles autonomously select radio resources for their V2V communications, without network assistance; this makes Mode 4 the baseline solution for safety applications. A description of its most significant attributes is provided next.

In Mode 4, C-V2X exploits a 10 or 20 MHz wide channel in the 5.9 GHz ITS band. It adopts Single-Carrier Frequency Division Multiple Access (SC-FDMA) with a fixed subcarrier spacing of 15 kHz. The basic frequency unit is a 180 kHz Resource Block (RB), while the time unit is a subframe whose duration is $t_s = 1$ ms.

Every time a vehicle has a packet to transmit, it encapsulates it within a TB; depending on its size, the TB is allocated over a variable number of frequency adjacent Resource Blocks (RBs) within the same subframe. Each TB also requires the transmission of the so-called Sidelink Control Information (SCI), that includes relevant elements for the

correct decoding of the TB, such as the adopted Modulation and Coding Scheme (MCS). The SCI is conveyed in the same subframe as its associated TB and it occupies 2 adjacent RBs.

In C-V2X Mode 4, vehicles autonomously select radio resources via the SSPS algorithm. Its procedure is fairly sophisticated (a thorough description of it is reported in [8] and [2]), but its outcome is the selection of a Single-Subframe Resource (SSR), defined as the set of RBs that allows to transmit a TB and its associated SCI; an SSR is exemplified in Fig. 1. In SSPS, the vehicle willing to transmit employs the channel status information gathered during the previous 1000 subframes, the so-called sensing window S, in order to learn which resources are reserved for future use by other vehicles. The building blocks of such long-term sensing are the SCIs received from near-by vehicles, the Received Signal Strength Indicator (RSSI) and the Reference Signal Received Power (RSRP) of every RB within the sensing window. During the selection window that opens up immediately afterwards, the vehicle exploits such knowledge to build a list of Candidate Subframe Resources (CSRs) among which the SSR for the transmission is randomly chosen. The selected time-frequency resources are periodically reserved for C_{resel} times, and after each transmission, the reselection counter C_{resel} is decremented by one. When the counter expires, a new resource selection procedure is triggered with probability $1-P$, $P \in [0, 0.8]$. The reservation interval P_{rsvp} between two consecutive transmissions matches the traffic period T. Further, the selection window duration W usually coincides with T, $W = T$. Fig. 1 visually summarizes the relevant elements of the SSPS algorithm.

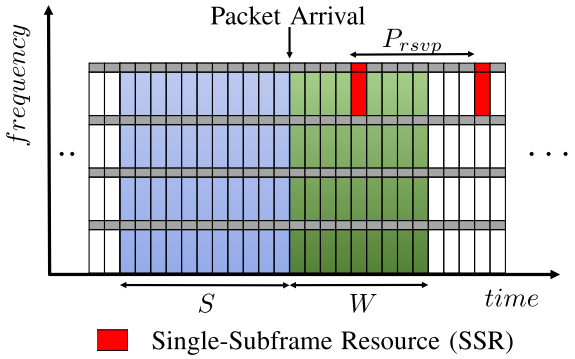

FIGURE 1. C-V2X resource grid arrangement.

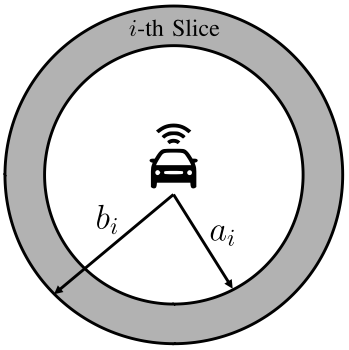

FIGURE 2. Generic slice.

B. PERFORMANCE METRICS

A merit figure that is widely adopted to measure the reliability of the SSPS algorithm, as well as of any alternative resource assignment technique, is the Packet Reception Ratio (PRR) [12]. For the i-th slice of distances from the generic, transmitting vehicle portrayed in Fig. 2, in which a_i and b_i are usually $a_i = i \cdot 20$ m, $b_i = (i+1) \cdot 20$ m, the PRR is evaluated as

$$PRR = \frac{\sum_{j=1}^{N} X_i^j}{\sum_{j=1}^{N} Y_i^j} \tag{1}$$

where X_i^j indicates the number of vehicles within the i-th slice that successfully receive the j-th packet, Y_i^j is the number of vehicles within the i-th slice and N denotes the number of packets generated during the simulation. The PRR is usually given as a function of the transmitter-receiver distance D, $PRR(D)$, where for the i-th slice $D = \frac{a_i+b_i}{2}$. Note that the SSPS strategy natively guarantees a bounded delay to packet transmissions, hence any investigation centered on such radio access strategy focuses on the PRR. The higher its values, the better. This is the variable to maximize, in order to reach the objective to increase as much as possible the probability that vehicles successfully receive the packets broadcasted by other vehicles.

The Channel Busy Ratio (CBR) is a further, interesting parameter, that reflects the load insisting on the channel. In [19], the CBR is defined as the fraction of subchannels in the resource pool whose Sidelink-Received Signal Strength Indicator (S-RSSI) measured by the vehicle exceeds a given threshold over subframes $[n-100, n-1]$.

The Packet Inter-Reception (PIR) is a performance metric useful for those use cases that require high reliability. It is defined as follows: for a given distance D, PIR is the time between two consecutive successful receptions of packets belonging to the same application flow, when the distance between the transmitting and receiving vehicle is within the $(0, D]$ range at the reception time of the two packets. The average PIR, $\overline{PIR}$, within a given distance D, is then computed as

$$\overline{PIR} = \frac{1}{M} \cdot \sum_{j=1}^{M} T_j \,, \tag{2}$$

where M denotes the number of collected PIR values during the simulation and T_j indicates the generic PIR value.

Last performance indicator considered is C_R, the Resource Block (RB) collision ratio, that in the m-th subframe is evaluated as the ratio between the number of RBs where a collision occurs and the number of occupied RBs, denoted by $collRB_m$ and $detRB_m$, respectively. The collision is defined as the event when two or more vehicles transmit on the same radio resource, causing a reciprocal interference that prohibits the correct decoding of their RBs. The average collision ratio is then computed over the number M of simulated

subframes as

$$\overline{C_R} = \sum_{m=1}^{M} \frac{collRB_m}{detRB_m}. \tag{3}$$

IV. SERVING APERIODIC TRAFFIC

A. THE PROPOSED SOLUTION

In this study, we put forth a reservation-less policy for the allocation of aperiodic traffic within the time-frequency grid described in Subsection III-A. We assume that aperiodic and periodic traffic coexist and that vehicles transmitting periodic traffic implement the usual SSPS algorithm.

We further suppose that all aperiodic TBs are characterized by the same Packet Delay Budget (PDB), corresponding to the maximum latency their delivery can tolerate, given by N_t ms. We require that every vehicle generating aperiodic traffic monitors the channel with no interruptions; for doing so, the vehicle continuously slides forward its sensing window S and updates the information collected through the received SCIs, the RSSI and the RSRP values. When the aperiodic TB is ready for transmission, the vehicle relies on the most recent sensing window to build its own, current view of the available SSRs, as if it were to transmit periodic traffic. In our proposal however, the vehicle applies the SSPS algorithm with a selection window whose duration is exactly $W = N_t$ ms, in order to respect the PDB; if more candidate SSRs are present, the resource selection is random, in line with the original algorithm. Moreover, the vehicle sets the reselection counter C_{resel} to 0, i.e., it places no periodic reservation, as if it were to perform a one-shot communication. The previous steps are then repeated for every aperiodic packet transmission. It follows that the vehicle only keeps track of the ongoing periodic reservations that it can hear, and that its aperiodic transmission does not conflict with them. Besides, when the aperiodic TB is sent over the air, its SCI also carries the $C_{resel} = 0$ indication; hence, all vehicles in radio visibility learn that the resources occupied by the aperiodic TB transmission will be freed up from next subframe onward. This implies that such vehicles build their own map of available resources taking into account ongoing periodic traffic only, monitoring its reservations, as it correctly has to be.

B. LIMITING ANALYSIS

It is now instructive to focus on the limiting condition when periodic traffic is absent and the previous strategy is employed to accommodate aperiodic traffic. In this scenario, we model the selection window as an $N_f \times N_t$ grid, where N_t represents the number of subframes in W, and N_f the number of RBs in the frequency channel. Next, we observe that: (i) the sensing window is useless here, owing to the lack of periodic reservations; (ii) the resource access policy is totally random. Let us further assume that the aperiodic traffic is Poisson distributed, with an overall average arrival rate given by λ TB/s, and that every TB plus the associated SCI requires the assignment of R RBs within a subframe, where for the sake of simplicity N_f is a multiple integer of R. If we neglect transmission impairments, that is, consider ideal transmission conditions, the evaluation of the aggregate aperiodic throughput $\mathcal{S}_{ap}$ is brought back to multi-channel slotted Aloha, where the number of channels is $\frac{N_f}{R}$. As a matter of fact, define G as the average number of aperiodic TBs collectively generated within a subframe of duration t_s, i.e.,

$$G = \lambda \cdot t_s\,, \tag{4}$$

In the simple case where $N_f > 1$ and $N_t = 1$, observe that the vulnerable period of the access strategy coincides with the subframe duration; indeed, all aperiodic TBs generated during a subframe will be transmitted within the next subframe. It readily follows that $\mathcal{S}_{ap}$ is given by

$$\mathcal{S}_{ap} = \left(\frac{N_f}{R}\right) \cdot \left(\frac{G}{\frac{N_f}{R}} \cdot e^{-\frac{G}{\frac{N_f}{R}}}\right) = G \cdot e^{-\frac{G}{\frac{N_f}{R}}}. \tag{5}$$

When $N_t > 1$, i.e., when the Selection Window is made of N_t consecutive subframes, the transmission attempts of aperiodic TBs generated during a given subframe are equally distributed over the next N_t subframes, each being subject to a Poisson traffic whose rate is $\lambda_i = \frac{\lambda}{N_t}$. On any subframe, this term adds to other $N_t - 1$ Poisson flows, originated within the previous N_t subframes, with every of them exhibiting a rate $\lambda_i = \frac{\lambda}{N_t}$. That is to say, the traffic poured on each of the N_t subframes is still Poisson, with rate $\sum_{i=1}^{N_t} \lambda_i = N_t \cdot (\frac{\lambda}{N_t}) = \lambda$, leading to the conclusion that, when $N_f > 1$ and $N_t > 1$, the aperiodic throughput $\mathcal{S}_{ap}$ is still given by (5).

This outcome is interesting, as (5) evidences that the aperiodic traffic throughput heavily depends on the size of aperiodic packets: for a given N_f value, the larger the size, the worse. Moreover, it is even more illuminating to observe that $\mathcal{S}_{ap}$ does not depend on N_t, i.e., on how stringent (or loose) the Packet Delay Budget PDB of aperiodic packets is. Pairing last result with the remark that aperiodic TBs will not collide with ongoing periodic traffic, as outlined at the end of previous subsection, allows to infer that the overall throughput of aperiodic and periodic traffic is insensitive to the delay requirement on the delivery of aperiodic packets. Ultimately, the PRR is expected to be independent of such PDB and indeed, the numerical results presented in Section V corroborate this insight.

If N_f is not a multiple integer of R, then the number of available channels is $\lfloor \frac{N_f}{R} \rfloor$, which forces some radio resources in a subframe to be unused. Their number amounts to $U = N_f - \lfloor \frac{N_f}{R} \rfloor \times R$. For a generic R, it follows that (5) modifies in

$$\mathcal{S}'_{ap} = \frac{N_f - U}{N_f} \cdot \left(G \cdot e^{-\frac{G}{\left\lfloor \frac{N_f}{R} \right\rfloor}}\right) < \mathcal{S}_{ap}. \tag{6}$$

The two previous expressions reveal that the choice of the R value plays a non-negligible role in the throughput evaluation. The emerging guideline is to adopt a proper combination of

packet size, MCS and code rate, to minimize U and therefore confine unused radio resources.

V. PHY LAYER FRAMEWORK

A. SIMULATIVE APPROACH

To model the PHY layer effects on the performance of the proposed algorithm in the most realistic manner, the custom ns-3 module operates on every received TB through two distinct numerical phases:

1. the average Signal-to-Interference-to-Noise Ratio (SINR) of the TB is determined;
2. the TB is declared successfully (or unsuccessfully) decoded, on the basis of look-up tables that report the Packet Error Rate (PER) for different average SINR values.

For the evaluation of the average SINR in phase 1, adhering to [12] the V2V channel is modeled through two states, Line of Sight (LOS) and Non-Line of Sight (NLOS). The latter state accounts for the presence of vehicles between the transmitting and receiving pair; its occurrence probability is a function of the distance between the two vehicles. In the LOS state, the path loss PL of the V2V link is evaluated as

$$PL = 32.4 + 20log_{10}(d) + 20log_{10}(fc) + L \qquad (7)$$

where d is the distance between the two vehicles, f_c denotes the center frequency in GHz, and L is a random term that models the shadowing, lognormally distributed with standard deviation $\sigma = 3$ dB. In the NLOS state, the path loss exhibits an additional random blockage term, still lognormally distributed, with a nonzero mean and $\sigma = 4.5$ dB [12].

It is further assumed that:

(i) the generic vehicle broadcasts messages with a transmission power equal to 23 dBm;
(ii) the noise power spectral density is equal to -174 dBm/Hz;
(iii) the receiver sensitivity is -90.4 dBm.

All these choices being set, the average SINR of the received TB can be evaluated.

In phase 2, the computed average SINR is mapped into a PER value that accounts for fast fading effects. The mapping relies on curves that have been newly obtained, as illustrated in next Subsection. Finally, the TB under examination is declared successfully decoded with probability $1-p$, whereas the TB decoding process fails with probability p; for a given average SINR, p is the corresponding PER value.

B. ERROR MODEL

The development of the ns-3 module has thoroughly covered each layer of the C-V2X protocol stack, for both data and control, leading to a final tool whose usage is computationally intensive. In order to confine some of its complexity, we decided to resort to the Link-to-System Mapping technique [20]: hence, the PER versus average SINR curves have been derived via separate link-level simulations. We have determined such curves from scratch, using MATLAB and its 5G toolbox, modeling the features of the transmitted signal and of the V2V channel so as to replicate the PHY layer choices expected to be standardized in 3GPP Release 16. Specifically, the short-term fading that affects the received signal has been modeled through two alternative Clustered Delay Lines (CDLs) [12], corresponding to the LOS and NLOS states mentioned above.

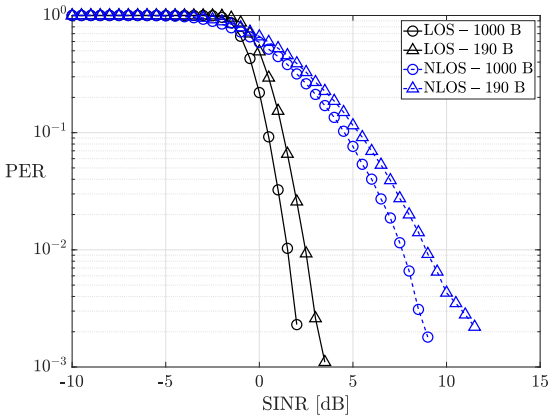

(a) TB

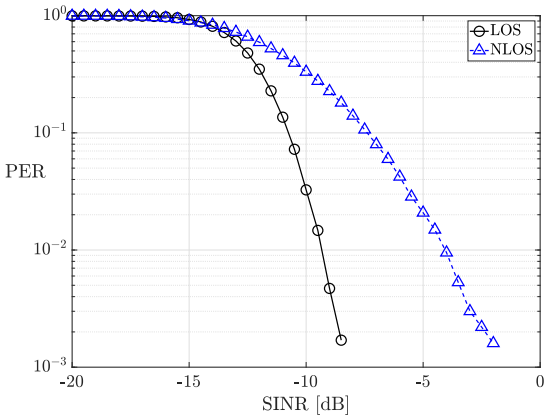

(b) SCI

FIGURE 3. PER as a function of the average SINR.

In MATLAB, the simulation of the TB transmissions on the V2V link exploits the Physical Sidelink Shared CHannel (PSSCH). The latter employs CP-OFDM, QPSK modulation and an LDPC code with rate 0.7; as specified in [12], 2×2 MIMO antennas are considered and no Hybrid ARQ is introduced. As for the SCI, the corresponding bits are transmitted resorting to the Physical Sidelink Control Channel (PSCCH) and they are protected by a polar code with rate 0.13. Moreover, the SCI content is redundantly transmitted over two adjacent RBs to improve robustness; accordingly, it is sufficient to correctly decode one RB out of the two to retrieve the SCI.

Fig. 3(a) reports the PER versus SINR curves we have numerically determined for the TBs, in the LOS and NLOS scenarios. The results have been obtained considering 10^4 samples and show that the LOS case is by far more favorable. Interestingly, when the TB size increases from 190 to

1000 bytes, the figure reveals that the performance slightly improves. This is is explained by the adoption of an LDPC code, exhibiting better performance for higher TB sizes, as reported in [21]. It is also valuable to note that these NR-V2X PER curves are qualitatively similar to those presented in [22], although they are not directly comparable, given different values of the system parameters and a different channel model are considered.

The PER curves for the SCI are shown in Fig. 3(b), demonstrating that the control information can be recovered at very low SINRs, in both LOS and NLOS conditions. These curves have then been translated into look-up tables and fed to the ns-3 simulator error model, resulting in a reduced computational load, while guaranteeing a very good accuracy level.

VI. NUMERICAL RESULTS

The results presented hereafter have been derived using the custom ns-3 C-V2X module originally developed by the authors in [8]. The simulator significantly enhances the original D2D module provided in [23] and features all the elements which are peculiar of C-V2X Mode 4 communications, accurately reflecting Release 14 standard solution. The following domains have been affected by the software development: the communication channel model, the PHY layer and the MAC sublayer. Contrary to [8], where dynamic traffic conditions were not introduced, this work accounts for vehicular mobility and models it through SUMO [24]. In accordance to the highway scenario defined in [12], the examined setting consists of a 4 km long highway trunk, where six 4 meter wide lanes are considered, three per each traveling direction. Vehicles travel on the lanes following the modified Krauss model [24]; their maximum speed is 140 km/h. The highway trunk has been populated considering three vehicular density values, 0.06, 0.12 and 0.26 vehicles/m, giving rise to three distinct scenarios that from now on will be termed low, medium and high density, respectively.

Vehicles generate application-layer packets in accordance to periodic and aperiodic traffic patterns; each packet is encapsulated within a single TB. Vehicles that act as periodic traffic sources generate 190 byte-long TBs every $T = 100$ ms. The Packet Delay Budget (PDB) of periodic traffic coincides with the period T. Vehicles acting as aperiodic traffic sources broadcast packets with an interarrival time τ given by

$$\tau = c + r \tag{8}$$

where c is a constant and r is an exponentially distributed random variable. This choice is in accordance to the aperiodic traffic models specified in [12]. The PDB of aperiodic packets coincides with c. Unless otherwise stated, in what follows $c = \bar{r} = 50$ ms. This implies that every vehicle generates packets at an average rate of 10 packets/s. Two alternative choices for the aperiodic packet size are considered: large or small packets, 1000 or 190 byte long, in order to better highlight the influence of this parameter on system performance.

TABLE 1. Simulation parameters.

Parameter	Values
Traffic density	10, 20, 43 vehicles/km/lane
Highway length	4 km
Number of lanes	6 (3 per driving direction)
Maximum speed	140 km/h
Periodic traffic Tx Frequency	10 Hz
Aperiodic traffic percentage (Δ)	0, 10, 50 and 90 %
Packet size (X)	190 bytes, 1000 bytes
Occupied subchannels	1 (190 bytes), 4 (1000 bytes)
Subchannel size	12 RBs
Channel bandwidth	10 MHz
Transmission power	23 dBm
Receiver sensitivity	-90.4 dBm
Modulation and coding scheme	QPSK 0.7

Vehicle radios operate at 5.9 GHz, on a 10 MHz channel that is partitioned in 4 subchannels of 12 RBs each. Both the 190B and 1000B TBs are transmitted assuming QPSK modulation with a 0.7 code rate, as indicated in Subsection V-B; they therefore occupy 1 and 4 subchannels, respectively.

As regards the algorithm ruling the radio resource allocation, it is SSPS for periodic traffic, with the reselection counter C_{resel} uniformly distributed in [5, 15]; further, in accordance to [4], the probability P is set to 0. Aperiodic traffic is served as indicated in Subsection IV-A.

Table 1 summarizes the most relevant numerical choices made in the current study.

The evaluation of the performance metrics introduced in Subsection III-B is presented next; for all results, an adequate number of simulations has been executed, in order to determine sufficiently tight 95% confidence intervals.

Figs. 4(a)-(c) report the PRR as a function of the transmitter-receiver distance D. The size of the aperiodic packets is $X = 1000$ bytes, different percentages of aperiodic traffic, namely, $\Delta = 10$, 50 and 90%, are considered, as well as the case when periodic traffic only is present ($\Delta = 0\%$). The worsening in performance for increasing Δ values is manifest. In the low density scenario, when half of the vehicles generate asynchronous traffic, the PRR drops below 0.9 for distances greater than 90 m. Moreover, Fig. 4(b) and Fig. 4(c) allow to appreciate how markedly the PRR worsens in increasingly crowded settings.

To better explain why the aperiodic traffic is so detrimental to the performance of SSPS, Table 2 reports the values of the Channel Busy Ratio (CBR) for the same choice of the parameters considered in Figs. 4(a)-(c). In this study, the S-RSSI threshold used to determine the CBR is equal to the receiver sensitivity level +0.5 dB; furthermore, the CBR is averaged over the central portion of the simulation time and over all vehicles. The first row of Table 2 refers to the low density scenario and reveals that the CBR monotonically increases from 0.45 to 0.72, when the percentage of aperiodic traffic raises from $\Delta = 0\%$ to $\Delta = 90\%$. Moving to the second and third row row of the Table, that is, considering the more crowded medium and high density settings, it is

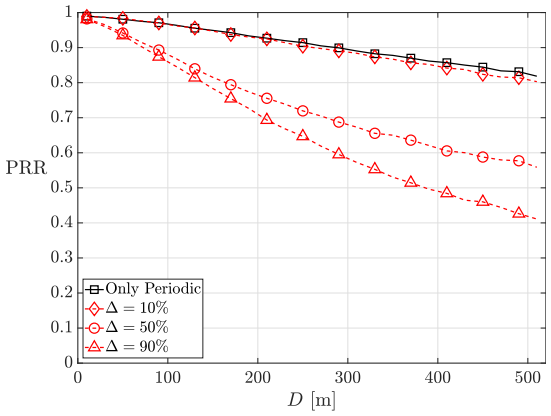

(a) Low density

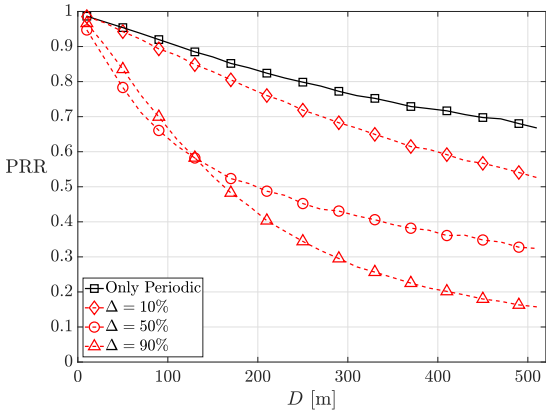

(b) Medium density

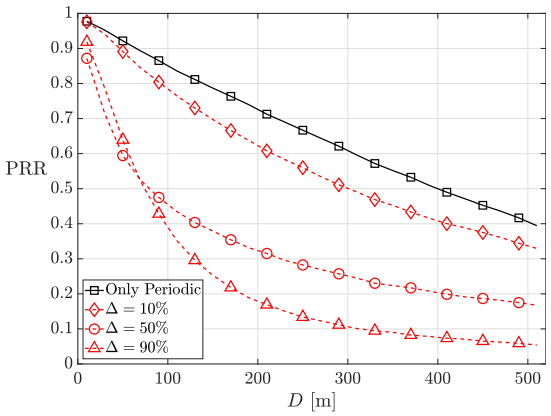

(c) High density

FIGURE 4. PRR as a function of the transmitter-receiver distance D, $X = 1000$ bytes.

observed that the CBR takes on notably high values. Overall, the combined effect of increased Δ values and increased vehicular densities leads to remarkable loads on the radio channel, that inflate the CBR and are responsible for the PRR degradation evidenced in Figs. 4(a)-(c). Table 3 also helps in grasping what happens in the medium and high density settings portrayed in Figs. 4(b) and (c). These figures revealed

TABLE 2. CBR values.

	$\Delta = 0\%$	$\Delta = 10\%$	$\Delta = 50\%$	$\Delta = 90\%$
Low density	0.44	0.49	0.55	0.72
Medium density	0.77	0.72	0.67	0.83
High density	0.92	0.93	0.75	0.88

TABLE 3. $\overline{C}_R$ values.

	$\Delta = 0\%$	$\Delta = 10\%$	$\Delta = 50\%$	$\Delta = 90\%$
Low density	0.11	0.14	0.19	0.22
Medium density	0.2	0.23	0.32	0.28
High density	0.32	0.35	0.46	0.4

that, for transmitter-receiver distances lower than 100 m, the PRR values for $\Delta = 50\%$ and $\Delta = 90\%$ are similar, with a slightly worse performance observed for $\Delta = 50\%$, in spite of a lighter load placed on the channel. The table discloses that the average collision ratio exhibits its maximum exactly for $\Delta = 50\%$ and that this maximum is not so far from the value observed for $\Delta = 90\%$ (0.32 versus 0.28 for the medium density scenario, 0.46 versus 0.4 for the high density scenario). When comparing the two cases, it is observed that for $\Delta = 50\%$ the aperiodic traffic is lighter, but the large, aperiodic packets randomly compete to gain access over a smaller fraction of radio resources left unoccupied by periodic flows, whose transmissions are protected by the proposed strategy. Conversely, the overall traffic is heavier for $\Delta = 90\%$, yet more radio resources are available for aperiodic transmissions. Ultimately, this leads to a PRR deterioration that is comparable in the two cases.

Figs. 5(a)-(c) are the counterparts of Figs. 4(a)-(c), when the size of the periodic packets is reduced to $X = 190$ bytes, all other system choices being unmodified. As it had to be expected, the size plays a relevant role in the achievable performance. Small aperiodic packets occupy a limited amount of radio resources, making the coexistence with periodic transmissions almost unproblematic. In the low density scenario, the PRR curves obtained for a small aperiodic packet size and different percentages of aperiodic traffic reveal a modest dependence on Δ. Further, the curves always lie in the region of the (D, PRR) plane where the PRR takes on values higher than 0.75. The curves obtained for different Δ values begin to differentiate at medium traffic density. The difference in the relative position of the curves referring to $\Delta = 0$, $\Delta = 10\%$ and $\Delta = 50\%$ in Fig. 5(a) (low density scenario) with respect to Fig. 5(b) (medium density scenario) can be understood observing that: (i) higher Δ values, i.e., higher percentages of aperiodic traffic, more heavily penalize the aperiodic flows PRR; (ii) in the medium density scenario, the number of aperiodic flows increases. Overall, this explains why, in Fig. 5(b), the overall PRR more markedly decreases moving from $\Delta = 0$ to $\Delta = 10\%$ and $\Delta = 50\%$ than it does in Fig. 5(a). When the extreme, high density landscape is examined, the curves are very far apart from one another and the PRR sharply degrades to unbearable values.

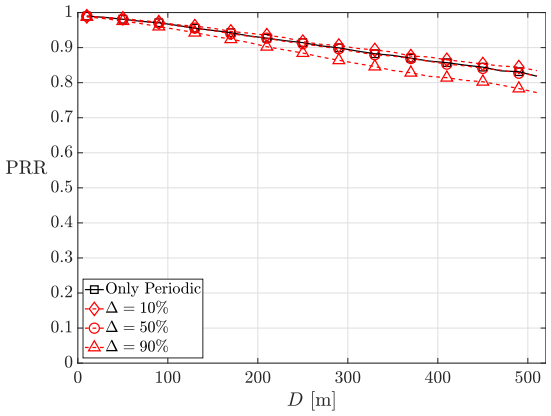

(a) Low density

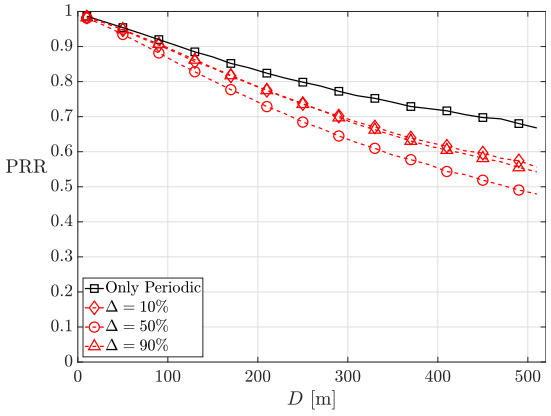

(b) Medium density

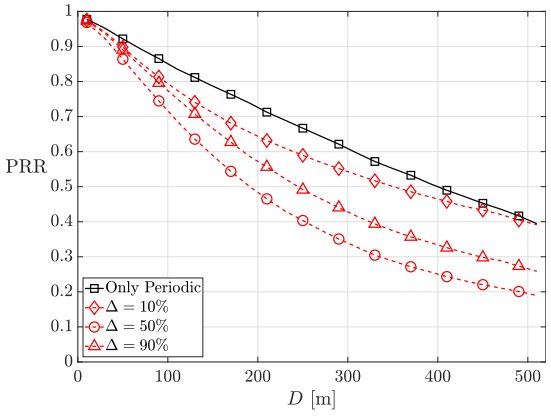

(c) High density

FIGURE 5. PRR as a function of the transmitter-receiver distance D, $X = 190$ bytes.

Unfortunately, aperiodic packets bred by general purpose eV2X applications are expected to exhibit a large size [12]. Unless otherwise stated, in what follows the main focus will therefore be on the attainable performance when relatively large-sized aperiodic packets ($X = 1000$ bytes) are considered. Moreover, the low density setting only will be examined.

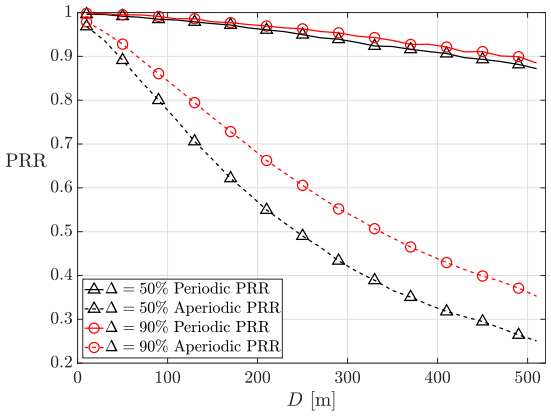

FIGURE 6. Aperiodic and periodic PRR as a function of D.

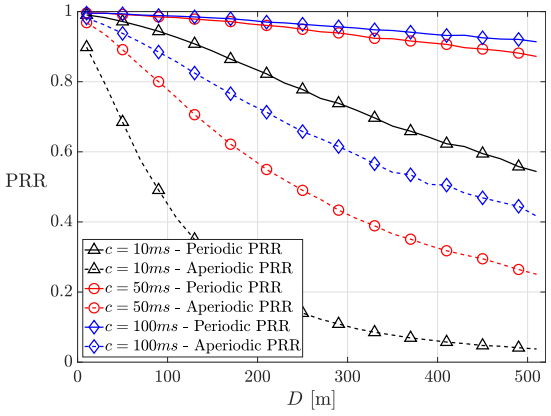

FIGURE 7. PRR for different aperiodic traffic models.

For the same system parameters considered so far, Fig. 6 separately reports the PRR experienced by vehicles generating periodic and aperiodic traffic as a function of the transmitter-receiver distance D, when $\Delta = 50\%$ and 90%. It is observed that: (i) the PRR of periodic traffic is almost unaffected by Δ; (ii) the PRR of aperiodic traffic is significantly worse than the PRR of periodic traffic and it decreases for increasing Δ. The reason is that an aperiodic vehicle performs a random resource selection contending with periodic and aperiodic traffic, but it respects periodic reservations. When Δ increases from 50% to 90%, the effect is emphasized, as aperiodic traffic requires four times the resources that periodic traffic asks for. When $\Delta = 50\%$, the aperiodic PRR is down to 0.8 at 130 m from the transmitting vehicle, revealing the low level of reliability guaranteed to the aperiodic packet delivery.

Fig. 7 delves into the impact that different arrival rates of aperiodic traffic have on the PRR of vehicles generating periodic and aperiodic packets. The results reported in this figure refer to $c = \bar{r} = 10$, 50 and 100 ms. The PDB of aperiodic packets is equal to 10, 50 and 100 ms, respectively. Note that the 10 and 50 ms choices adhere to the preliminary indications for eV2X applications detailed in [12]. The curves reveal that the PRR of both periodic and aperiodic traffic collapses when the arrival rate is significantly high.

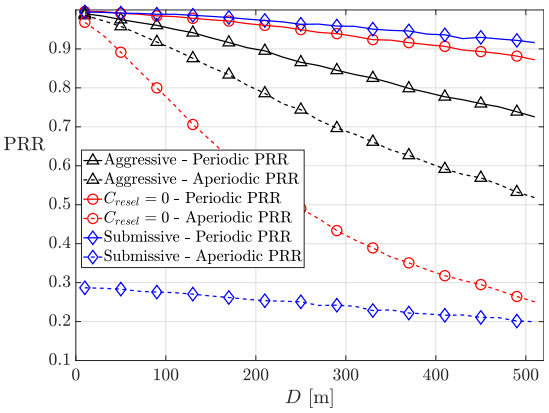

(a) $X = 1000$ Bytes

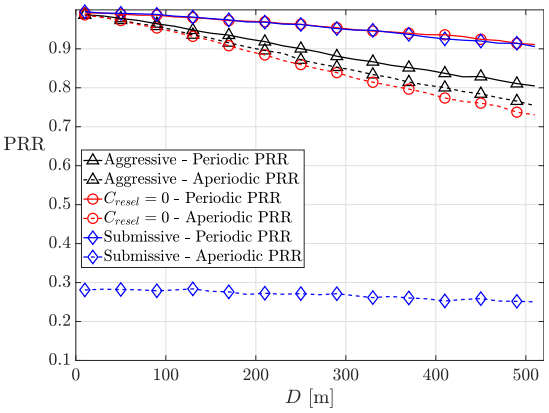

(b) $X = 190$ Bytes

FIGURE 8. Comparison among alternative schemes, $\Delta = 50\%$.

Next, in order to offer a further insight into the behavior of the proposed strategy for handling aperiodic traffic, such solution is compared against two schemes that accommodate aperiodic traffic in accordance to SSPS. We term such alternatives submissive and aggressive scheme and report their description below. For the submissive scheme, aperiodic traffic reserves radio resources strictly in accordance to SSPS, hence periodically, employing a reservation interval P_{rsvp} that matches the mean interarrival time of aperiodic packets. When an aperiodic packet is ready for transmission, the originating vehicle first checks if the next reserved radio resource becomes available within the packet delay budget of aperiodic traffic. If it does, the TB of the aperiodic packet plus its SCI are allocated within such resource. Otherwise, the aperiodic packet is dropped, as its transmission within the next reserved resource would violate the delay requirement. The aggressive scheme differs from the submissive scheme only in the event that next reserved resource violates the delay budget. In this circumstance, the aperiodic packet is not dropped; rather, the corresponding TB plus its SCI is transmitted over a free resource picked at random in a selection window W whose duration coincides with the aperiodic PDB. Both solutions represent interesting terms of comparison: the

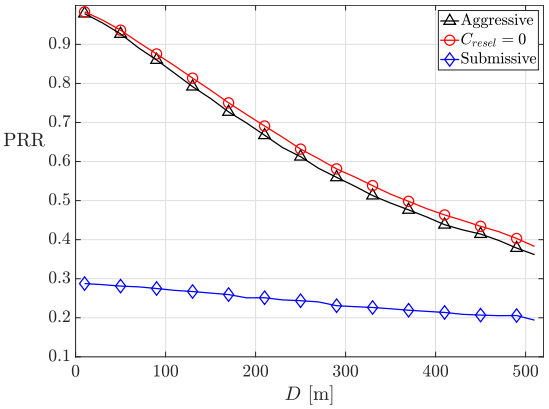

FIGURE 9. Comparison among alternative schemes, $\Delta = 100\%$ and $X = 1000$ bytes.

former does not prevaricate over periodic flows, as aperiodic traffic adheres to periodic reservations whenever possible and is dropped otherwise; on the other hand, the latter scheme always serves aperiodic traffic, at the expense of periodic traffic.

Hence, Fig. 8(a) compares the PRR of periodic and aperiodic traffic obtained when aperiodic packets gain access to the channel in accordance to our proposal (red curves) with the PRR performance achieved by the aggressive and the submissive strategy (black and blue curves, respectively). Here, $\Delta = 50\%$, $c = \bar{r} = 50$ ms and $X = 1000$ bytes. The submissive scheme penalizes aperiodic traffic to a great extent, while the aggressive scheme heavily strikes on periodic traffic performance. On the other hand, our solution serves periodic packets in an excellent manner at the expense of aperiodic traffic, resulting in an intermediate approach. For the sake of completeness, Fig. 8(b) broadens the comparison, considering $X = 190$ bytes. For this size of aperiodic packets, the submissive strategy is inadequate too, whereas our solution overall performs better than the aggressive scheme. The PRR that our proposal guarantees periodic packets is as high as possible, while the PRR of aperiodic packets is only slightly lower than the PRR aperiodic traffic experiences if the aggressive strategy is adopted. To complete the comparison, Fig. 9 confronts our proposal, the submissive and aggressive strategies, when $\Delta = 100\%$ and $X = 1000$ bytes. As somewhat had to be expected, in this limiting case, the submissive strategy is largely unsuccessful, whereas the performance of the aggressive scheme gets close to our proposed solution.

Next, Fig. 10 reports the overall PRR as a function of the transmitter-receiver distance D for different values of the PDB of the aperiodic traffic, $PDB = 10, 20, 30$ and 50 ms, for $\Delta = 50\%$, $c = \bar{r} = 50$ ms and $X = 1000$ bytes. The figure shows that the PDB choice has no impact on the PRR curves, confirming the *a priori* indication provided by the throughput analysis in Subsection IV-B. The effect of more stringent delay requirements for aperiodic traffic is to shrink its selection window W; this might lead to the erroneous intuition that, for a given traffic density, a PDB decrease

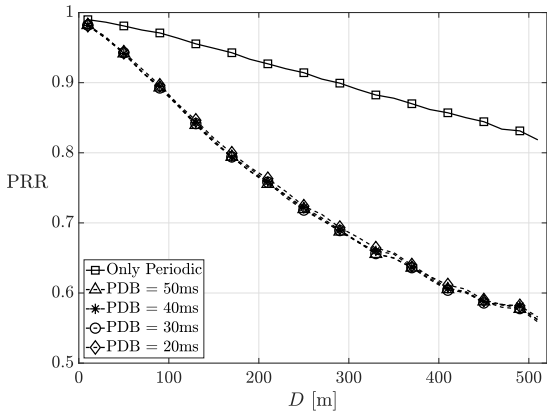

FIGURE 10. PRR for different values of the packet delay budget.

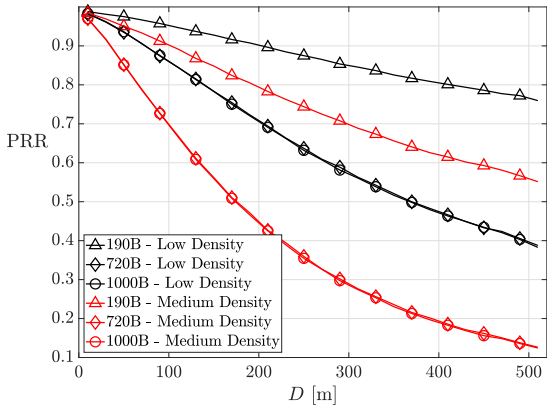

FIGURE 11. PRR when $\Delta = 100\%$.

should reflect in a lower PRR. However, Fig. 10 demonstrates it is not true.

Fig. 11 considers the limiting case when only aperiodic traffic is present ($\Delta = 100\%$), and reports the PRR for three values of packet size, $X = 1000$, 720 and 190 bytes, when the low and medium density scenarios are examined. The PER curves for the new value of packet size, $X = 720$ bytes, have been obtained but not explicitly reported, as they are very similar to those referring to $X = 1000$ bytes in Fig. 3. On one hand, increasing the packet size from $X = 190$ to 720 bytes has a remarkable negative effect on the PRR. The effect is amplified the more crowded the vehicular setting is. On the other hand, the PRR is not affected at all by the packet size increase from $X = 720$ to 1000 bytes. As a matter of fact, the PRR depends on the maximum number of packets that can be successfully allocated without collisions in every subframe, which is expressed by the ratio between the number of available subchannels and the number of required subchannels for packet. Such ratio specializes to $\lfloor \frac{4}{1} \rfloor$ when $X = 190$ bytes, and to the same unitary value for $X = 720$ and $X = 1000$ bytes, $\lfloor \frac{4}{3} \rfloor$ and $\lfloor \frac{4}{4} \rfloor$, respectively. More generally, if larger packet sizes not fitting in one subchannel were to be considered, it is our belief that fragmentation should be avoided. Rather, a more spectrally efficient modulation scheme might be used; depending on the application type and on its requirements, a low code rate might also be employed.

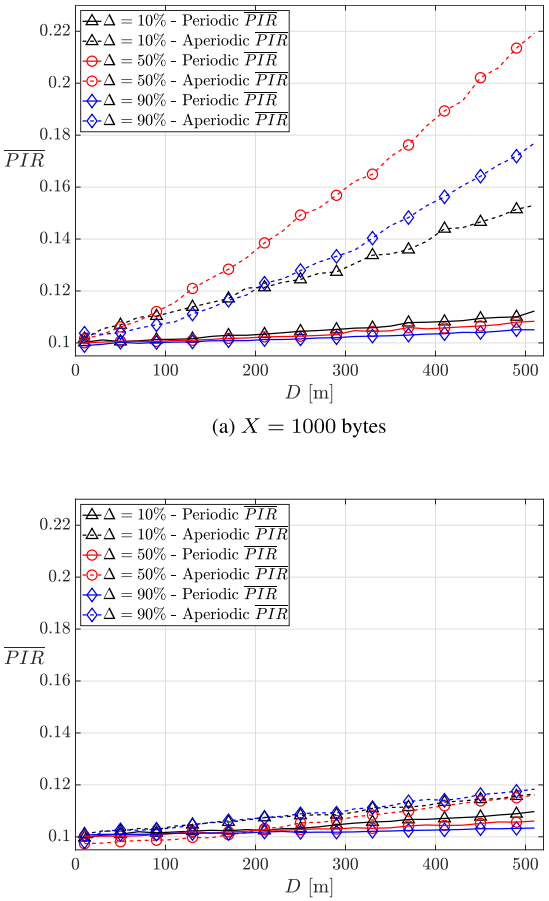

(a) $X = 1000$ bytes

(b) $X = 190$ bytes

FIGURE 12. Average PIR of aperiodic and periodic traffic as a function of D.

In Fig. 12(a), the average Packet Inter-Reception $\overline{PIR}$ as a function of D is separately reported for aperiodic and periodic traffic in the low density scenario, for $\Delta = 10\%$, 50% and 90% and $X = 1000$ bytes. The same remarks applied to Fig. 6 hold, as the average PIR strongly depends on the PRR: when the former lowers, the latter inevitably climbs up. In Fig. 12(b), the same setting is considered, except for the packet size, which is $X = 190$ bytes; as already observed with reference to Fig. 5(a), the injection of aperiodic traffic is not problematic, as long as the size of its packets is small.

Fig. 13 concludes the investigation, reporting the PIR Cumulative Distribution Function (CDF) for periodic and aperiodic traffic flows, for $\Delta = 10\%$, 50% and 90% in the low density scenario, when $X = 1000$ bytes. In this figure, $D = 520$ m; the CDF is therefore evaluated from the PIR values collected for all transmitter-receiver distances falling in the (0, 520] range. The PIR CDF of periodic traffic exhibits a step behavior, that reflects the periodicity $T = 100$ ms of resource assignment; note that these curves are nearly independent on the aperiodic traffic percentage. Instead, the PIR CDF of aperiodic traffic smoothly varies, reflecting that aperiodic traffic is characterized by a random inter-packet arrival time and is randomly served. Unfortunately, this figure

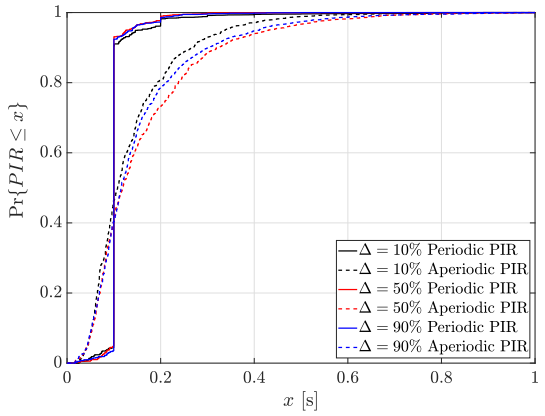

FIGURE 13. Aperiodic and periodic PIR CDF, $X = 1000$ bytes.

demonstrates that the PIR of aperiodic traffic cannot be successfully confined: the probability of observing PIR values lower than 100 ms is only 0.4, unbearable for all future eV2X use cases.

VII. CONCLUSION

The current work has studied the coexistence of aperiodic and periodic traffic in Mode 4. A reservation-less Mode 4 variant for serving aperiodic packets has been put forth, and its behavior has been analytically modeled in the limiting condition where aperiodic traffic only is present. A custom ns-3 C-V2X module and a 5G-compliant PHY error model have been newly developed, and the impact of different percentages and arrival rates of aperiodic flows, size of aperiodic packets and vehicular densities on system performance has been quantified through extensive simulations.

The obtained results demonstrate that the PRR and PIR of aperiodic traffic are insensitive to different latency requirements set for aperiodic packets. The paper also reveals that it is arduous to guarantee aperiodic packets good performance levels for any of the examined traffic densities, if relatively large sized aperiodic packets are considered. It therefore indicates that Mode 4 long-term sensing cannot be uncritically inherited by the forthcoming 5G NR-V2X technology to support high reliability and confined delay services. As a matter of fact, higher NR numerologies will help in reducing latencies, but the efficient allocation of aperiodic traffic still awaits for the final answer. It is the authors' viewpoint that among the various MAC proposals for Release 16, TFRPs or geographic information-based dynamic mapping can mainly mitigate inefficiencies due to the hidden terminal problem and to the half-duplex constraint. On the other hand, short-term sensing represents an appealing solution, that deserves further investigations.

REFERENCES

[1] European Telecommunications Standards Institute, *Intelligent Transport Systems (ITS); Vehicular Communications; Basic Set of Applications; Specification of Cooperative Awareness Basic Service*, document ETSI EN 302 637-2 V1.3.1, Sep. 2014.

[2] R. Molina-Masegosa and J. Gozalvez, "System level evaluation of LTE-V2 V mode 4 communications and its distributed scheduling," in *Proc. IEEE 85th Veh. Technol. Conf. (VTC Spring)*, Sydney, NSW, Australia, Jun. 2017, pp. 1–5.

[3] A. Bazzi, G. Cecchini, A. Zanella, and B. M. Masini, "Study of the impact of PHY and MAC parameters in 3GPP C-V2 V mode 4," *IEEE Access*, vol. 6, pp. 71685–71698, 2018.

[4] M. Gonzalez-Martin, M. Sepulcre, R. Molina-Masegosa, and J. Gozalvez, "Analytical models of the performance of C-V2X mode 4 vehicular communications," *IEEE Trans. Veh. Technol.*, vol. 68, no. 2, pp. 1155–1166, Feb. 2019.

[5] C. Campolo, A. Molinaro, F. Romeo, A. Bazzi, and A. O. Berthet, "Full duplex-aided sensing and scheduling in cellular-V2X mode 4," in *Proc. 1st ACM MobiHoc Workshop Technol., mOdels, Protocols for Cooperat. Connected Cars (TOP-Cars)*, Catania, Italy, 2019, pp. 19–24.

[6] CAR 2 CAR Communication Consortium, *Survey on ITS-G5 CAM Statistics*, document TR2052, V1.0.1, Dec. 2018.

[7] R. Molina-Masegosa, M. Sepulcre, J. Gozalvez, F. Berens, and V. Martinez, "Empirical models for the realistic generation of cooperative awareness messages in vehicular networks," *IEEE Trans. Veh. Technol.*, vol. 69, no. 5, pp. 5713–5717, May 2020.

[8] L. Gibellini and M. L. Merani, "Out-of-Coverage multi-hop road safety message distribution via LTE–A cellular V2 V (C-V2 V)," in *Proc. IEEE 88th Veh. Technol. Conf. (VTC-Fall)*, Chicago, IL, USA, Aug. 2018, pp. 1–6.

[9] F. Romeo, C. Campolo, A. Molinaro, and A. O. Berthet, "DENM repetitions to enhance reliability of the autonomous mode in NR V2X sidelink," in *Proc. IEEE 91st Veh. Technol. Conf. (VTC-Spring)*, Antwerp, Belgium, May 2020, pp. 1–5.

[10] Z. Zhou, H. Yu, C. Xu, Y. Zhang, S. Mumtaz, and J. Rodriguez, "Dependable content distribution in D2D-based cooperative vehicular networks: A big data-integrated coalition game approach," *IEEE Trans. Intell. Transp. Syst.*, vol. 19, no. 3, pp. 953–964, Mar. 2018.

[11] Z. Zhou, F. Xiong, C. Xu, Y. He, and S. Mumtaz, "Energy-efficient vehicular heterogeneous networks for green cities," *IEEE Trans. Ind. Informat.*, vol. 14, no. 4, pp. 1522–1531, Apr. 2018.

[12] 3GPP, Sophia Antipolis, France, *Study on Evaluation Methodology of New Vehicle-to-Everything (V2X) Use Cases for LTE and NR*, Rel-15 V15.3.0, 3GPP, document TR 37.885, Jun. 2019.

[13] 3GPP, Sophia Antipolis, France, *Enhancement of 3GPP Support for V2X Scenarios*, Rel-16 V16.2.0, 3GPP, document TS 22.186, Jun. 2019.

[14] 3GPP, Sophia Antipolis, France, *Overall Description of Radio Access Network (RAN) Aspects for Vehicle-to-Everything (V2X) Based on LTE and NR*, Rel-16 V1.0.0, 3GPP, document TR 37.985, Nov. 2019.

[15] 3GPP, Sophia Antipolis, France, *Sidelink resource allocation Mode 2 for NR-V2X*, 3GPP, document R1-1911884, TSG RAN WG1 Meeting #99, Nov. 2019.

[16] Fifth Generation Communication Automotive Research and Innovation, *Final 5G V2X Radio Design*, 5GCAR Deliverable D3.3 v1.0, May 2019, pp. 62–70.

[17] 3GPP, Sophia Antipolis, France, *Geographic Information based Dynamic TFRP Resource Selection Procedure in NR-V2X*, document R1-1905375, 3GPP TSG RAN WG1 Meeting #96b, Apr. 2019.

[18] 3GPP, Sophia Antipolis, France, *Dynamic Resource Selection for NR Sidelink*, document R1-1913273, 3GPP TSG RAN WG1 Meeting #99, Nov. 2019.

[19] 5G Automotive Association, *V2X Functional and Performance Test Procedures - Selected Assessment of Device to Device Communication Aspects*, 5GAA, Munich, Germany, Oct. 2018.

[20] M. Mezzavilla, M. Miozzo, M. Rossi, N. Baldo, and M. Zorzi, "A lightweight and accurate link abstraction model for the simulation of LTE networks in ns-3," in *Proc. 15th ACM Int. Conf. Modeling, Anal. Simulation Wireless Mobile Syst. (MSWiM)*, Paphos, Cyprus, 2012, pp. 55–60.

[21] D. Hui, S. Sandberg, Y. Blankenship, M. Andersson, and L. Grosjean, "Channel coding in 5G new radio: A tutorial overview and performance comparison with 4G LTE," *IEEE Veh. Technol. Mag.*, vol. 13, no. 4, pp. 60–69, Dec. 2018.

[22] W. Anwar, N. Franchi, and G. Fettweis, "Physical layer evaluation of V2X communications technologies: 5G NR-V2X, LTE-V2X, IEEE 802.11bd, and IEEE 802.11p," in *Proc. IEEE 90th Veh. Technol. Conf. (VTC-Fall)*, Honolulu, HI, USA, Sep. 2019, pp. 1–7.

[23] R. Rouil, F. J. Cintron, A. B. Mosbah, and S. Gamboa, "Implementation and Validation of an LTE D2D Model for ns-3," in *Proc. Workshop ns-3*, Porto, Portugal, Jun. 2017, pp. 1–6.

[24] P. A. Lopez, E. Wiessner, M. Behrisch, L. Bieker-Walz, J. Erdmann, Y.-P. Flotterod, R. Hilbrich, L. Lucken, J. Rummel, and P. Wagner, "Microscopic traffic simulation using SUMO," in *Proc. 21st Int. Conf. Intell. Transp. Syst. (ITSC)*, Maui, HI, USA, Nov. 2018, pp. 2575–2582.

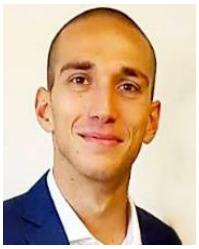

LUCA LUSVARGHI (Graduate Student Member, IEEE) received the master's degree *(summa cum laude)* in electronics engineering from the University of Modena and Reggio Emilia, Italy, in July 2019. He is currently pursuing the Ph.D. degree with the Department of Engineering "Enzo Ferrari," International ICT Doctorate School. His research interest includes 5G technologies, particularly on cellular vehicle-to-everything (C-V2X) communications. He is also the Developer and a Maintainer of the C-V2X open-source ns-3 module employed in this work.

MARIA LUISA MERANI (Senior Member, IEEE) is currently with the Department of Engineering, University of Modena and Reggio Emilia, Italy, where she is also an Associate Professor. She has published her textbook *Hands-On Networking: From Theory to Practice* (Cambridge University Press, October 2009) and in the same year she was one of the authors of the book *Handbook of P2P Networking* (Springer, 2009). Her research interest includes wireless networking. She has served as the Technical Program Co-Chair for the 2nd IEEE International Symposium on Wireless Communication Systems 2005 (ISWCS 2005) and IEEE Globecom, 2007 and 2009 editions. In 2010, she was the General Chair of the Fifth Edition of the IEEE International Symposium on Wireless Pervasive Computing. She has served as an Editor for the IEEE TRANSACTIONS ON WIRELESS COMMUNICATIONS.